EurJIC
European Journal of Inorganic Chemistry

A Journal of ChemPubSoc Europe

Accepted Article

Title: The template-free synthesis of CuO@CeO2 nanospheres: facile strategy, structure optimization, and enhanced catalytic activity toward CO oxidation

Authors: Yunfei Su, Shanshan Yuan, Dandan Ning, Qingwen Zhang, Weiliang Han, and Yi Wang

To be cited as: *Eur. J. Inorg. Chem.* 10.1002/ejic.201800348

Link to VoR: http://dx.doi.org/10.1002/ejic.201800348

WILEY-VCH

10.1002/ejic.201800348

WILEY-VCH

The template-free synthesis of CuO@CeO_2 nanospheres: facile strategy, structure optimization, and enhanced catalytic activity toward CO oxidation

Yunfei Su [a,b], Shanshan Yuan[a,b], Dandan Ning[a,b], Qingwen Zhang[a,b], Weiliang Han[c] and Yi Wang*[a,b]

Abstract: The template-free construction of hollow-multiporous materials with hierarchically multiporous wall, unique morphology and functionality remains a great challenge in materials science. Here we describe a facile template-free approach to synthesize hollow-multiporous wall CeO_2 (HMW-CeO_2) nanospheres. The HMW-CeO_2 nanosphere possesses hierarchically multiporous wall, with pores size ranging from micropores to mesopores, centred at 0.43, 4.2 and 14.3 nm. The CuO loaded HMW-CeO_2 support (HMW-CuO@CeO_2) was evaluated for the catalytic activity in the CO oxidation reaction. The HMW-CuO@CeO_2 exhibited highest catalytic activity than that of other CeO_2 catalysts. The results show low T_{100} of about 60 °C (temperature at which 100% CO conversion has been achieved) and high stability with negligible decrease of CO conversion during 12h reaction. Overall, it provides a simple, low cost and mass-productive method for the preparation of highly active catalysts for CO oxidation.

Introduction

Ceria (CeO_2) plays an important role as a catalyst which supports in a variety of catalytic reactions, due to its excellent redox properties and high oxygen storage capacity.[1-8] The properties of ceria in turn are associated with arrangement of the terminated surface oxygen atoms, greatly depend on the morphology, structure and component. Generally, there are two strategies to enhance ceria catalytic activity, including the optimization of ceria morphologies/structure and the combine of ceria with secondary species, such as noble metals or metal oxides, to form composites.[9-13] For the first strategy, numerous morphologies/structures of ceria have been designed, such as nanorods,[14] nanotubes,[15] nanosheaths,[16] nanobundles,[17] mesoporous,[18] cage-bell[19] and other morphologies/structures.[20] In addition, the relationship between morphologies/structures and their catalytic properties have been extensively studied as well. Especially, the structure with high surface area, for instance, a mesoporous structure conducive to the secondary components diffusion and expose more active facets in the catalytic reaction. Furthermore, the mesoporous structure is also favorable for the diffusion and adsorption of reactant molecules. For the second strategy, although noble metals are able to improve the catalytic activity of ceria, the high cost, limited availability, and low resistance to halogens greatly restrict their large-scale application. However, because of the synergistic effect, some of ceria-based bimetal oxides show perfect catalytic activity compared with noble metal-based catalysts in specific catalytic reactions.[21] Furthermore, the ceria-based bimetal oxides catalyst is cheaper than the noble metal-based catalyst. Therefore, the construction of ceria-based bimetal oxides with high surface area could take full advantages of two strategies stated above, and thus is of particular interest to optimize their catalytic activities.

As one of the important ceria-based bimetal oxides, CuO@CeO_2 systems have drawn continuous attention because of their highly enhanced catalytic performance and low price, especially in CO catalytic oxidation.[14, 18, 22] So far, the CuO@CeO_2 catalysts have been prepared by the methods of precipitation,[23] pregnation[24] and sol-gel.[25] But, it is hard to synthesize small size of particles with high specific surface area and high porosity according to above methods. In order to increase the surface area of CuO@CeO_2 catalysts, template method has been employed, such as polymer template,[26] silica template[27] and carbon template.[28] For example, Shi et al. prepared mesoporous CuO@CeO_2 by a two-step approach, in which CeO_2 was first synthesized via hard template method followed by etching off mesoporous silica KIT-6 template by NaOH solution, and then CuO was loaded into the CeO_2 through impregnation method.[29] Our research group has continuously focused on the CuO@CeO_2 catalyst toward CO catalytic oxidation. We also prepared mesoporous CuO@CeO_2 catalyst via hard template.[30, 31] The CuO@CeO_2 catalyst exhibited a perfect catalytic activity for CO oxidation with the T_{50} (the temperature when the conversion was 50%) of only 34 °C. Unfortunately, the construction of mesoporous CuO@CeO_2 catalyst by template methods are usually time consuming and costly due to the requirement for the synthesis of the template and the multi-step templating process. Therefore, it is meaningful to develop an effective and facile method for the synthesis of large scale CuO@CeO_2 catalyst with optimized structure, high surface area, highly catalytic activity and stability .

Herein, we report a facile, low cost and robust approach for the synthesis of nanospheres aggregates CuO@CeO_2 catalyst with hollow-multiporous wall (HMW) structure. The whole synthetic process is showed schematically in Fig.1. 1) The ceria alkoxide nanosphere (A) was prepared by mixing $Ce(NO_3)_3$, isopropanol and glycerol. 2) The nanosphere A was undergone with hydrothermal reaction and calcination which resulted in the formation of HMW structured CeO_2 nanosphere (B, HMW-CeO_2). 3) CuO was loaded into the CeO_2 to form HMW-CuO@CeO_2 (C).

[a] Y.F. Su, S. S. Yuan, D.D. Ning, Q.W. Zhang, Prof. Y. Wang
School of Ophthalmology and Optometry, Eye Hospital, School of Biomedical Engineering
Wenzhou Medical University
E-mail: wangyi@wibe.ac.cn
[b] Y.F. Su, S. S. Yuan, D.D. Ning, Q.W. Zhang, Prof. Y. Wang
Wenzhou Institute of Biomaterials and Engineering
Chinese Academy of Sciences
Wenzhou, 325000, China
[c] Prof. W.L. Han
Lanzhou Institute of Chemical Physics
Chinese Academy of Sciences
Lanzhou, 730000, China

Importantly, there are no organic/inorganic templates and/or additives added in the whole synthetic process. In addition, as compared with CeO_2 catalyst produced by conventional template-assisted methods, our method provides the formation of the HMW-CuO@CeO_2 catalysts with relatively lower density, high surface area and highly stable structure without the destructive effect upon template removal during sythesis. Furthermore, the CO catalytic activity of HMW-CuO@CeO_2 catalyst was significantly enhanced. Although we have focused on the CuO@CeO_2 catalyst here, the template-free method can be easily extended to synthesize other HMW structures, such as, NiO@CeO_2, Co_3O_4@CeO_2 and Fe_3O_4@CeO_2 oxides composites. Therefore, the synthetic method can potentially be scaled up for industrial production.

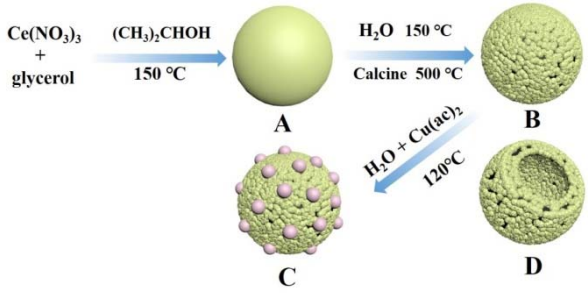

Fig.1 Synthesis of CuO@CeO_2 Hollow-Multiporous Wall nanospheres.

Results and Discussion

Here we demonstrated a facile template-free approach to synthesize the hollow-multiporous wall CuO@CeO_2 (HMW-CuO@CeO_2) nanospheres. To investigate the unexpected morphology evolvement from ceria alkoxide nanospheres to HMW-CeO_2 nanospheres, a time-dependent experiment was carried out based on TEM measurement (Fig. S1). At the beginning of the hydrothermal reaction, the ceria alkoxide nanosphere was a full sphere (Fig. S1a). After about 60 min reaction, some pore structures were formed on the surface of sphere, while the ceria alkoxide nanosphere was consumed (Fig. S1b). After 180 min, the ceria alkoxide nanosphere was completely consumed with the formation of HMW-ceria hydroxide nanosphere (Fig. S1c). Eventually, HMW-CeO_2 nanosphere was obtained after calcination treatment of HMW-ceria hydroxide nanosphere at 500 °C for 3h (Fig. S1d). The template-free method formation of the hollow-multiporous wall structure could be explained by the Kirkendall effect.[32] A similar hollowing phenomenon was also observed in the Co system.

The phase purity and crystal structure of the ceria alkoxide nanosphere, HMW-CeO_2 and HMW-CuO@CeO_2 (12 mol%) were examined by XRD. As shown in Fig. 2, the HMW-CeO_2 after calcinations at 500 °C exhibits higher crystallinity than that of the ceria alkoxide nanosphere. By comparing the XRD pattern of the standard CeO_2 sample (JCPDS PDF#43-1002), it was judged that the HMW-CeO_2 and HMW-CuO@CeO_2 (12 mol%) have a typical crystalline fluorite structure. The average size of crystalline HMW-CeO_2 and HMW-CuO@CeO_2 (12 mol%) is 4.9

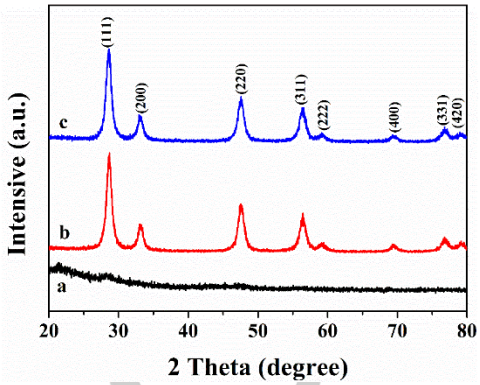

Fig.2 Wide-angle XRD patterns of (a) ceria alkoxide nanosphere, (b) HMW-CeO_2, (c) HMW-CuO@CeO_2 (12 mol%).

nm and 5.1 nm, respectively, calculated from line broadening of the ceria (111) plane using Scherrer's formula. The results suggest that CeO_2 particles are composed of nanocrystal subunits. There are no other peaks identified, indicating that the samples have good phase purity. The absence of copper oxide diffraction peaks from HMW-CuO@CeO_2 (12 mol%) suggests that the copper species are highly dispersed or incorporated in the ceria lattice. The results are consistent with our previous work.[18] Fig. S2 shows the FTIR spectra of the HMW-CeO_2 nanosphere and ceria alkoxide nanosphere. For all samples, the peaks centered at about 1620 and 3360 cm^{-1} are assigned to the hydroxyl groups of the superficial adsorbed or crystallized water. For the HMW-CeO_2 nanosphere, the other peaks in the range of 500-2000 cm^{-1} are related to Ce-O.[33] For the ceria alkoxide nanosphere, the peaks located below 2000 cm^{-1} are generally assigned to Ce-O, C-C, C-C-O and C-O-Ce groups. The similar FTIR results were also observed previously for other metal alkoxides[34]. The peak intensity of the Ce-O bond for HMW-CeO_2 nanosphere is different from ceria alkoxide nanosphere, indicated that the structure of the HMW-CeO_2 nanosphere has a little distinction with ceria alkoxide nanosphere.

The size, morphology and pore structure of the HMW-CeO_2 were examined by SEM and TEM measurements, as shown in Fig.3. From the SEM images (Fig.3a and b), the HMW-CeO_2 nanopheres show uniform spherical shape, with an average size of about 500 nm. Their hollow structures are clearly seen through some broken nanospheres in Fig. 3b. In addition, it is clear from Fig. 3b that the HMW-CeO_2 nanophere displays multiporous wall structure. The hollow structure and multiporous wall structure of HMW-CeO_2 nanopheres are further confirmed by the TEM images, as shown in Fig.3c, d and e. This structure is almost the same as the expected model shown in Fig.1. The selected-area electron diffraction (SAED) patterns are given in Fig. 3f. There are multiple bright electron diffraction rings, indicating the generation of polycrystalline HMW-CeO_2. To investigate the elemental distribution of Ce and Cu in the hollow-multiporous wall nanosphere, the TEM-mapping was employed. The elemental mapping images (Fig. S3) show that Ce and Cu elements are uniformly distributed on the whole hollow-multiporous wall nanosphere. This kind of uniform elemental

distribution is absolutely favorable for the interaction between CeO_2 and CuO.

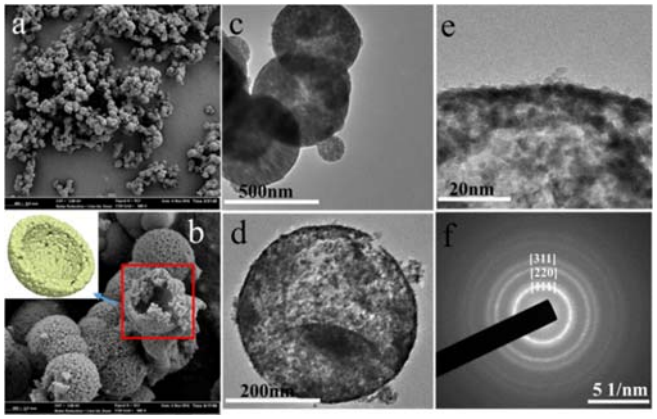

Fig.3 (a) and (b) are SEM images of the HMW-CeO_2 nanosphere (c), (d) and (e) are TEM images of the HMW-CeO_2 nanosphere, (f) is the SAED pattern of HMW-CeO_2 nanosphere.

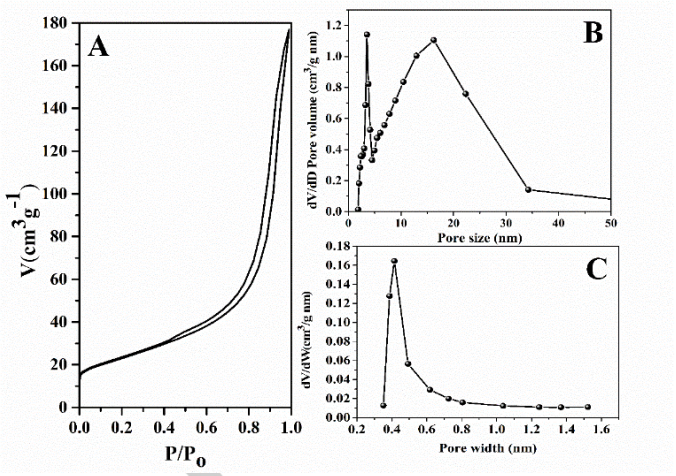

Fig.4 N_2 adsorption analysis of HMW-CeO_2 (A) N_2 adsorption-desorption isotherms, (B) BJH pore size distribution and (C) Horvath-Kawazoe pore size distribution from N_2 adsorption isotherm for HMW-CeO_2.

The porous structure and surface area of HMW-CeO_2 nanospheres were investigated by N_2-adsorption measurements, as shown in Fig. 4A. A H_2 type hysteresis loop could be observed in the P/P_0 range of 0.4–0.995 for the HMW-CeO_2 nanosphere. The isotherm exhibited type IV behaviors, indicating the presence of mesoporous structure in the HMW-CeO_2 nanospheres. A hysteresis loop at a higher pressure (P/P_0 = 0.90–0.995) may reflect presence of a macroporous structure, which is related to the formation of HMW-CeO_2. The pore size distribution calculated by Barrett-Joyner-Halenda (BJH) model (Fig. 4B) and Horvath-Kawazoe model (Fig. 4C) are distinct maxima centered at 0.43, 4.2 and 14.3 nm, indicating that the HMW-CeO_2 nanosphere is hierarchically multiporous wall structure. The textural properties of HMW-CeO_2 obtained from the N_2-isotherms are summarized in Table S1. The BET surface area and pore volume are calculated to be as high as 101 m^2g^{-1} and 0.37 cm^3g^{-1}, respectively. After supported with 12 mol% CuO (Fig. S4 and Table S1), the BET surface area of HMW-CuO@CeO_2 is decreased from 101 to 90 m^2g^{-1}, the pore volume is decreased from 0.37 to 0.31 cm^3g^{-1}, which is possibly due to the partial pore blocking by the introduction of CuO.

The catalytic oxidation of CO have an important role in addressing some of the major industrial applications such as catalytic combustion for CO removal from vehicle exhaust, end-pipe gases, fuel cell and many other applications[7, 9]. The morphologies/structure plays an important role in CO catalytic oxidation. The nano-CeO_2 and meso-CeO_2 were prepared in our previous work, and the complete conversion temperature (T_{100}) was about 185 and 135 °C for the CO oxidation, respectively.[7,18] Compared with nano-CeO_2 and meso-CeO_2, the HMW-CeO_2 showed the best CO catalytic activity in this work, and the T_{100} was about 115 °C. It is indicated that the hollow-multiporous wall structure of HMW-CeO_2 is relatively conducive to the CO oxidation. But good performance of CO catalytic oxidation is only observed at much higher temperatures. The catalytic activity can be further enhanced through addition of CuO, the obtained HMW-CuO@CeO_2 catalyst with different CuO contents were evaluated for their performance in the catalytic CO oxidation reaction, and the results are shown in Fig. 5A. With an increase of the reaction temperature, the catalytic activities in the CO oxidation become better. The light-off temperature of CO (T_{100}, temperature at which 100% CO conversion has been achieved) decreases in the following order for HMW-CuO@CeO_2 catalysts: HMW-CuO@CeO_2 (24 mol%) > HMW-CuO@CeO_2 (18 mol%) > HMW-CuO@CeO_2 (6 mol%) > HMW-CuO@CeO_2 (12 mol%). The catalytic activity of all HMW-CuO@CeO_2 catalysts was better than HMW-CeO_2 catalyst, the T_{100} of HMW-CuO@CeO_2 (12 mol%) was achieved at around 60 °C. Considering the excellent catalytic activity and simple preparation method, the HMW-CuO@CeO_2 (12 mol%) might also be exploited for practical application in gas sensors or breathing-protection masks. To investigate the stability of the HMW-CuO@CeO_2 catalyst, the HMW-CuO@CeO_2 (12 mol%) was employed as a typical example toward CO oxidation reaction continuously examined for 12 h (Fig. 5B). It can be noticed a stability test with a long period is studied for HMW-CuO@CeO_2 (12 mol%) catalyst, and the catalytic activity unchanged before 12h and have slight loss (about 2%) of CO conversion is observed after 12 h on stream at 60 °C. It is due to the sintering of CuO species on the surface of HMW-CuO@CeO_2 (12 mol%) catalyst. It's worth mentioning that, the BET surface area and pore volume of HMW-CuO@CeO_2 (12 mol%) after the stability testing are calculated to be as high as 89 m^2g^{-1} and 0.30 cm^3g^{-1}, respectively (Fig. 5C and Table S1). The result show that the HMW-CuO@CeO_2 (12 mol%) is well to maintain its hollow hierarchically multiporous wall structure after catalytic reaction.

The information of surface composition and chemical state of the synthesized catalysts was studied by XPS. Fig. 6A gives the Ce 3d spectra of the HMW-CeO_2 and HMW-CuO@CeO_2 (12 mol%) catalysts. Two principal peaks for Ce ($3d_{5/2}$, $3d_{3/2}$) and four

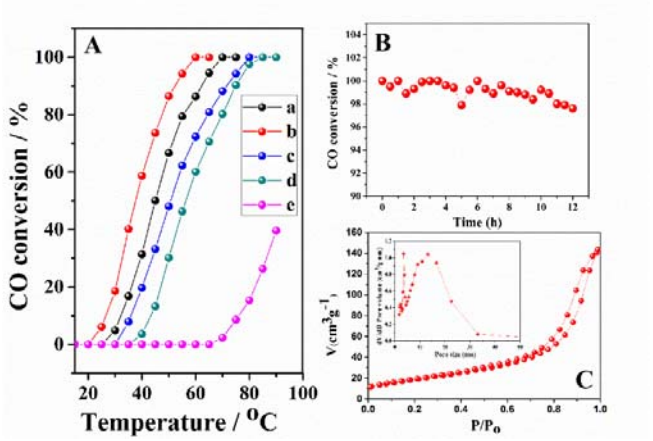

Fig. 5 (A) CO conversion as a function of temperature for (a) HMW-CuO@CeO_2 (6 mol%), (b) HMW-CuO@CeO_2 (12 mol%), (c) HMW-CuO@CeO_2 (18 mol%) , (d) HMW-CuO@CeO_2 (24 mol%) and (e) HMW-CeO_2. (B) The stability testing of HMW-CuO@CeO_2 (12 mol%) catalyst measured at 60 °C for catalytic oxidation under the condition of (A). (C) N_2 adsorption-desorption isotherms and BJH pore size distribution of HMW-CuO@CeO_2 (12 mol%) catalyst after the stability testing.

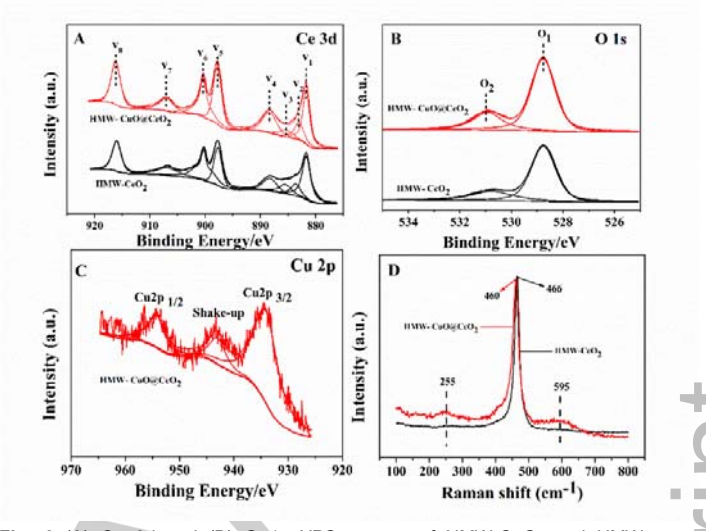

Fig. 6 (A) Ce 3d and (B) O 1s XPS spectra of HMW-CeO_2 and HMW-CuO@CeO_2 (12 mol%), (C) Cu 2p XPS spectra of HMW-CuO@CeO_2 (12 mol%). (D) Raman spectra of HMW-CeO_2 and HMW-CuO@CeO_2 (12 mol%).

satellites marked by asterisks are associated with the Ce (IV) $4f^0$ initial state of CeO_2. According to previous literature[35], the six peaks (V_1, V_4, V_5, V_6, V_7, V_8) are characteristic of the Ce^{4+} 3d final states and the two peaks (V_2, V_3) are characteristic of the Ce^{3+} 3d final states. The phenomenon show that a mixture of Ce^{3+}/Ce^{4+} oxidation states exists on the surface of two samples, and the result was in good agreement with the studies reported by He et al[36]. The calculated percentages of Ce^{3+} can be determined by Ce^{3+}/ (Ce^{3+} + Ce^{4+}), as listed in Table S2. It is worthy to note that the percentage of Ce^{3+} in HMW-CuO@CeO_2 (12 mol%) catalyst is higher than HMW-CeO_2 catalyst, suggesting that more oxygen vacancies are present in HMW-CuO@CeO_2 (12 mol%) catalyst. The reason is that Cu ions incorporated into the ceria lattice leads to the increase of defective sites and oxygen vacancies (O:) in the structure. Surface Cu molar percentage derived from XPS for HMW-CuO@CeO_2 (12 mol%) catalyst is listed in Table S2. It can be seen that the Cu molar ratio obtained from XPS result is lower than the initial Cu molar ratio. The reason is that the XPS can only quantify the Cu content on the surface of the HMW-CuO@CeO_2 (12 mol%) catalyst while the amount of Cu in the pore is not included. The XPS O 1s spectra for the HMW-CeO_2 and HMW-CuO@CeO_2 (12 mol%) were also examined (Fig. 6B). The one (O_1) with lower binding energy is assigned to lattice oxygen in the metal oxides, the other (O_2) with higher binding energy is ascribed to chemisorbed oxygen and weakly bonded oxygen species on the surface of samples.[37] The calculated percentages of active O_2 (chemisorbed oxygen) percentage can be determined by O_2 / (O_1 + O_2), and results are listed in Table S2. It is noticed that the support of Cu species can effectively enhance the chemisorbed oxygen on the surface of the HMW-CuO@CeO_2 (12 mol%) catalyst. Fig. 6C shows the Cu 2p binding energy of HMW-CuO@CeO_2 (12 mol%) catalyst. Accordingly, the Cu ($2p_{3/2}$, $2p_{1/2}$) peaks at around 934.1 and 954.2 eV with shake-up structure at 940–945 eV in the spectra can only be attributed to Cu(II) ions[27]. For HMW-CeO_2, the electronic structure has a direct impact on the redox capacity, since the formation of oxygen vacancies, the primary ionic defects, is accompanied by electron redistribution to render the system charge neutral. Specifically, the formation of an oxygen vacancy is accompanied by electron localization in the unoccupied 4f orbitals of two Ce^{4+}. Using Kroger-Vink notation, the point defect reaction is given by: $O^{2-}+2Ce^{4+}\rightarrow V_O+2Ce^{3+}+1/2\ O_2$ (V_O is oxygen vacancy).[38]This sample further studied by performing Raman spectroscopy measurements, as shown in Fig. 6D. The HMW-CeO_2 catalyst exhibits the characteristic F_{2g} vibration band at about 466 cm^{-1}.[39] Once copper species is introduced, this peak shifts from 466 to 460 cm^{-1}, and becomes broader and weaker.The reason of shifting and broadening may be ascribed to the presence of oxygen vacancies, which is related to structural defects derived from partially incorporation of copper into CeO_2 lattice. In addition, two weak peaks center at about 255 and 595 cm^{-1} are ascribed to oxygen vacancies, and the amount of oxygen vacancy can be reflected by the peak area at 255 and 595 cm^{-1}. The larger the peak area is, the more oxygen vacancy a catalyst can have[40]. Compared with HMW-CeO_2, there are more oxygen vacancies of the HMW-CuO@CeO_2 (12 mol%) due to the incorporation of copper.

In addition, H_2-TPR is employed as an effective tool to investigate the reducibility of the catalysts and determine their capability to remove or take up oxygen. The reduction of pure HMW-CeO_2 is evidenced by three weak reduction peaks at 330, 520 and 800 °C and should be attributed to the reduction of surface oxygen and bulk oxygen, respectively,[39] as shown in Fig. 7A. A H_2 consumption peak at about 330 °C was observed in the pure CuO sample that was synthesized using a conventional precipitation method. The HMW-CuO@CeO_2 shows two overlapping reduction peaks in the temperature range of 220-280 °C, which is much lower than that of pure CuO. It has been

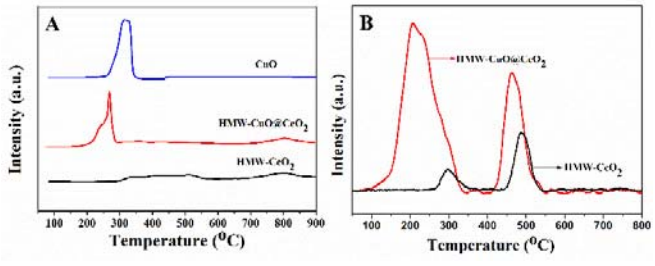

Fig. 7 (A) H_2-TPR profiles of HMW-CeO_2, HMW-CuO@CeO_2 (12 mol%) and CuO, (B) O_2-TPD profiles of HMW-CuO@CeO_2 (12 mol%) and HMW-CeO_2.

reported CeO_2 promotes the reduction of finely dispersed CuO surface species, and small CuO particles, are easier to be reduced.[41] Bulk CuO can be reduced at higher temperatures, but has a few contribution to catalytic activity. The HMW-CuO@CeO_2 shows relatively easy reducibility due to the better dispersion of Cu species, as indicated in the XRD and EDX-mapping results (Fig 2 and Fig S3). As compared with pure CuO, the reduction temperature of CuO species for HMW-CuO@CeO_2 is lower than that of pure CuO, indicating the strong interaction between CuO species and CeO_2, probably in the form of $CuCeO_x$ solid solution.[36] The Cu^{2+}-O^{2-}-Ce^{4+} connection in $CuCeO_x$ solid solution could reduce the redox potential of Cu species as well as act as a bridge for O transfer between Cu and Ce.[36] Therefore, the reducibility is enhanced due to strong interaction between Cu and Ce in the solid solution, and this allows having an effective redox cycle during oxidation reactions. The lower the reduction temperature is, the stronger the redox ability of a catalyst is. In addition, temperature programmed desorption of oxygen (O_2-TPD) to determine the mobility of oxygen species, as shown in Fig. 7B. According to the previously reported literature,[42] the oxygen species were desorbed from easiest to hardest as follows: oxygen molecule (O_2) > oxygen molecule anion (O_2-) > oxygen anion (O^-) > lattice oxygen (O^{2-}). O_2- is molecular adsorption oxygen and the O^- is surface chemical adsorption oxygen. They are belong to the surface active oxygens, and relatively easy to be desorbed from the metal oxide. It is extremely difficult for lattice oxygen to be desorbed from the metal oxide catalysts.[43,44] From Fig.7B, it can be seen that there are two obvious desorption peaks appeared. The first O_2 desorption peak occurred at lower temperature corresponds to the desorption of surface active oxygen (O_{sa}), such as O_2- and O^-, while the peak at higher temperature is owing to the desorption of surface lattice oxygen (O_{sl}).[45] Note that the O_{sa} peak intensity of HMW-CuO@CeO_2 is much higher than that of HMW-CeO_2, while the O_{sa} peak temperature of HMW-CuO@CeO_2 (210 °C) is lower than that of HMW-CeO_2 (300 °C). It is indicated that the HMW-CuO@CeO_2 surface has abundant surface active oxygen species. It is due to the strong interaction between CuO and CeO_2 across the interface.[14,16,] It is beneficial for oxygen in the gas phase to be activated and adsorbed onto the solid surface. The desorption temperature and intensity of catalysis is related to their catalytic activity.[46] The low beginning desorption temperature and high intensity of desorption peaks, are the meaning of high catalytic ability of a catalyst. Therefore, the better catalytic activity of HMW-CuO@CeO_2 is due to high amount of surface active oxygen species, which are involved easily participate in the catalytic oxidation reaction.

It is well known that the activity of a transition metal oxide catalyst is influenced by several factors, such as surface area, pore structure, and surface active oxygen.[47-49] According to the characterization results in the present study, the HMW-CeO_2 has the larger BET surface area (Fig 4 and Table S1), and has a special HMW structure (As shown by TEM). The larger surface area can ecpose more active facets in the oxidation reaction and a HMW structure is favourable for the adsorption and diffusion of reactants and products. It is worthy to note that the introduction of CuO species into CeO_2 could further promote the creation of oxygen vacancies at/or around the HMW-CuO@CeO_2 interface in the presence of an appropriate amount of CuO (As shown by Raman). As is known, at the presence of CuO-CeO_2 interaction, the addition of CuO on CeO_2 dramatically enhances the reducibility of surface-capping oxygen on CeO_2, promotes the bulk oxygen migration to the surface as well as the formation of active surface absorbed oxygen species and creates oxygen vacancies in the bulk region of CeO_2.[14,38,50] Cu ions incorporated into the ceria lattice can lead to the defective sites and oxygen vacancies (O:) in the structure of catalyst (i.e., xCuO + (1-x)CeO_2 → xCu_Ce^{2+} + xO: + (2-x)O^{2-} + (1-x)Ce_Ce^{4+}).[50] Oxygen vacancy is the active center, which promotes the dissociation of oxygen molecules into chemisorbed oxygen and thus facilitates the CO oxidation reaction. Furthermore, with the doping of copper, the oxygen vacancies are increased along with the improved catalytic activity for HMW-CuO@CeO_2 catalysts. However, an excessive amount of CuO doped into CeO_2 nanospheres may block the pore channel and hinder the active sites of CeO_2, which resulted in poorer catalytic activity. As a consequence, we conclude that the good performance of the HMW-CuO@CeO_2 catalyst was associated with the higher surface area and surface active oxygen concentration, better secondary species dispersion, and HMW structure. Moreover, we believe that this work provides a facile method for the synthesis of hollow multiporous catalysts including other composite materials with high catalytic activity.

Conclusions

In summary, we have shown that high-quality hollow-multiporous CuO@CeO_2 catalyst with hierarchically multiporous wall structure and textural parameters can be obtained through a low-cost and straightforward template-free approach. The prepared HMW-CuO@CeO_2 catalyst exhibited excellent long-term stability and high activity toward CO catalytic oxidation. The outstanding CO catalytic performance of HMW-CuO@CeO_2 catalyst is associated with components and structural parameters. This work demonstrates that a fine control over nanoscale structural features offers new perspectives for the catalyst design.

Experimental Section

2.1 Preparation of ceria alkoxide nanospheres

Ceria alkoxide nanospheres were synthesized by mixing $Ce(NO_3)_3{\cdot}6H_2O$, isopropanol and glycerol in a Teflon-lined stainless steel autoclave. In a typical synthesis, 0.868 g $Ce(NO_3)_3{\cdot}6H_2O$ was dissolved in 30 mL isopropanol and stirred for 30 min. 10 mL glycerol was added to the above solution and stirred for 30 min. And then, the mixture was transferred into a Teflon-lined stainless steel autoclave at 150 °C for 8 h. After cooling to room temperature naturally, the precipitate was filtrated, washed and dried at 80 °C to obtain ceria alkoxide nanosphere.

2.2 Preparation of hollow-multiporous wall CeO_2 (HMW-CeO_2)

HMW-CeO_2 was prepared by the hydrothermal reaction of ceria alkoxide nanosphere. Typically, 0.5 g ceria alkoxide nanosphere was added to the 30 mL deionized water and stirred for 20 min. And then, the mixture was transferred into a Teflon-lined stainless steel autoclave at 150 °C for 3 h. After cooling to room temperature naturally, the precipitate was filtrated, washed and dried at 80 °C and calcined at 500 °C to obtain HMW-CeO_2.

2.3 Preparation of hollow-multiporous wall CuO@CeO_2 (HMW-CuO@CeO_2)

The HMW-CuO@CeO_2 catalysts with different CuO content (6, 12, 18, 24 mol%) were prepared using a hydrothermal method. For a typical synthesis of HMW-CuO@CeO_2 (12 mol%), 0.139 g $Cu(CH_3COO)_2{\cdot}H_2O$ was dissolved in 30 mL of ultrapure water under stirring. And then the as-prepared HMW-CeO_2 was added to the above solution and stirred for 30 min. The obtained slurry was transferred into a Teflon-lined stainless steel autoclave at 120 °C for 12 h and cooled to room temperature naturally. Finally, the precipitate was filtrated, washed and dried at 80 °C to obtain HMW-CuO@CeO_2 (12 mol%).

2.4 Catalyst characterization

Powder X-ray diffraction (XRD) analysis was performed to verify the crystallographic phase present catalysts. XRD patterns of the samples were recorded on a Rigaku D/MAX-RB X-ray diffractometer with a target of Cu Kα operated at 60 kV and 55 mA with a scanning speed of 5° min^{-1}. The 2θ of wide-angle ranged from 20°-80° and the 2θ of low-angle ranged from 0.6° to 5°.

Transmission electron microscopy (TEM) experiments were measured on a JEOL JEM-2010 transmission electron microscope equipped with an Oxford energy-dispersive X-ray (EDX) spectrometer attachment operating at 200 kV.

The specific surface area and the mean pore diameter of the catalysts were determined by nitrogen adsorption in accordance with the BET method, meaured on Micromeritics 3Flex instrument. The BET surface area were determined based on six measurements at relative pressures of N_2 in the range of 0.05~1.00.

Fourier transform infrared spectroscope (FTIR, Nexus 870FT-IR) was used to record the FTIR spectra of the sample ranging from 400 to 4000cm^{-1}.

Chemical states of the atoms in the catalyst surface were investigated by X-ray photoelectron spectroscopy (XPS) on a VG ESCALAB 210 Electron Spectrometer (Mg Ka radiation; hv = 1253.6 eV). XPS data were calibrated using the binding energy of C1s (284.6 eV) as the standard.

H_2-TPR measurements were performed on online GC-7890II gas chromatograph equipped with a thermal conductivity detector (TCD). The reducing gas was 5 vol.% H_2 balanced by argon, and a flow rate of 40 ml·min^{-1} was used. The quartz tube reactor was loaded with 20 mg sample in powder form. The test was carried out from room temperature to 800 °C at a heating rate of 10 °C·min^{-1}. Before each measurement, the sample was purged with dry air at 400 °C for 1 h.

2.5 Measurements of catalytic performance

Catalytic activity tests were performed in a continuous-flow fixed-bed microreactor. A glass tube with an inner diameter of 6 mm was used as the reactor tube. About 150 mg catalyst with the average diameter of 20~40 mesh was placed into the tube. The reaction gas mixture consisted of 1 vol.% CO balanced with air was passed through the catalyst bed at a total flow rate of 50 mL·min^{-1}. A typical weight hourly space velocity (WHSV) was 10000 mL·g^{-1}·h^{-1}. The composition of the influent and effluent gas was detected with an online GC-7890II gas chromatograph equipped with a thermal conductivity detector. The CO conversion was calculated based on the outlet CO:

$$\text{Conversion of CO\%} = \frac{([CO]_{in} - [CO]_{out})}{[CO]_{in}} \times 100$$

The $[CO]_{in}$ and $[CO]_{out}$ was CO concentration (vol.%) in mixture gas before and after CO catalytic oxidation reaction, respectively.

Acknowledgements

Science&Technology Program of Wenzhou (G20160008), The National Natural Science Foundation of China (21605116),Public Projects of Zhejiang Province (2017C33193), Public Projects of Wenzhou (Y20160065, Y20160067), Wenzhou government's startup fund (WIBEZD2014004-02).

Keywords: Hollow-Multiporous Wall • synergistic effect • CuO@CeO_2 composites • CO oxidation

[1] K.R. Hahn, A.P. Seitsonen, M. Lannuzzi, J. Hutter, *ChemCatChem,* **2015**, 7, 625-634.

[2] S. Kumar, A. K. Ojha, D. Patrice, B. S. Yadav, A. Materny, *Phys. Chem. Chem. Phys.* **2016**,18, 11157-11167.

[3] L.J. Yan, Y.Y. Liu, K.W. Zha, H.R. Li, L.Y. Shi, D.S. Zhang, *ACS Appl. Mater. Inter.* **2017**, 9, 2581-2593.

[4] J. Roggenbuck, H. Schäfer, T. Tsoncheva, C. Minchev, J. Hanss, M. Tiemann, *Micropor. Mesopor. Mat.* **2017**, 101, 335-341.

[5] Q. Shen, M. Wu, H. Wang, C. He, Z. Hao, W. Wei, Y. Sun, *Catal. Sci. Technol.* **2015**, 5, 1941-1952.

[6] W. Shi, Y. Li, J. Hou, H. Lv, X. Zhao, P. Fang, F. Zheng, S. Wang, *J. Mater. Chem. A.* **2013**, 1, 728-734.

[7] Y. Su, Z. Tang, W. Han, P. Zhang, Y. Song, G. Lu, *CrystEngComm.* **2014**, 16, 5189-5197.

[8] K.W. Zha, S.X. Cai, H. Hu, H.R. Li, T.T. Yan, L.Y. Shi, D.S. Zhang, *J. Phys. Chem. C.* 2017, 121, 25243-25254.

[9] D. Gamarra, A. L. Cámara, M. Monte, S. B. Rasmussen, L. E. Chinchilla, A. B. Hungría, G. Munuera, N. Gyorffy, Z. Schay, V. C. Corberán, J. C. Conesa, A. Martínez-Arias, *Appl. Catal. B: Environ.* **2013**, 130-131, 224-238.

[10] C.H. Du, Y. Guo, Y.L. Guo, X.Q. Gong, G.Z. Lu, *J. Mater. Chem. A.* **2017**, 5, 5601-5611.
[11] S. Sun, D. Mao, J. Yu, Z. Yang, G. Lu, Z. Ma, *Catal. Sci. Technol.* **2015**, 5, 3166-3181.
[12] X.N. Hu, L. Huang, J. P. Zhang, H.R. Li, K.W. Zha, L.Y. Shi, D.S. Zhang, *J. Mater. Chem. A.* **2018**, 6, 2952-2963.
[13] X.Z. Cui, Y.X. Wang, L.S. Chen, J.L. Shi, *ChemCatChem.* **2014**, 6, 2860-2871.
[14] G. Chen, Q. Xu, Y. Yang, C. Li, T. Huang, G. Sun, S. Zhang, D. Ma, X. Li, ACS *Appl. Mater. Interfaces.* **2015**, 7, 23538-23544.
[15] C. Pan, D. Zhang, L. Shi, J. Fang, *Eur. J. Inorg. Chem.* **2012**, 2429-2436.
[16] X. Wang, Y. Zhang, S. Song, X. Yang, Z. Wang, R.Jin, H. Zhang, *Angew. Chem. Int. Ed.* **2016**, 55, 4542 –4546.
[17] R. Rao, M. Yang, C. Li, H. Dong, S. Fang, A. Zhang, *J. Mater. Chem. A.* **2015**, 3, 782-788.
[18] Y. Su, Z. Tang, W. Han, Y. Song, G. Lu, *Catal. Surv. Asia.* **2015**, 19, 68-77.
[19] H. Guo, Y. He, Y. Wang, L. Liu, X. Yang, S. Wang, Z. Huang, Q. Wei, *J. Mater. Chem. A.* **2013**, 1, 7494–7499.
[20] X. Wang, D. Liu, S. Song, H. Zhang, *J. Am. Chem. Soc.* **2013**, 135, 15864-15872.
[21] J. Shi, *Chem. Rev.* **2013**, 113, 2139-2181.
[22] J. Qin, J. Lu, M. Cao, C. Hu, *Nanoscale*. **2010**, 2, 2739-2743.
[23] L. Qi, Q. Yu, Y. Dai, C. Tang, L. Liu, H. Zhang, F. Gao, L. Dong, Y. Chen, *Appl. Catal. B: Environ.* **2012**, 119-120, 308-320.
[24] W.W. Wang, P.P. Du, S.H. Zou, H.Y. He, R.X. Wang, Z. Jin, S. Shi, Y.Y. Huang, R. Si, Q.S. Song, C.J. Jia, C.H. Yan, *ACS. Catal.* **2015**, 5, 2088-2099.
[25] S. Li, N. Wang, Y. Yue, G. Wang, Z. Zu, Y. Zhang, *Chem. Sci.* **2015**, 6, 2495-2500.
[26] Y. Zhang, H. Liang, X. Y. Gao, Y. Liu, *Catal. Comm*. **2009**, 10, 1432-1436.
[27] J. Zhu, Q. Gao, Z. Chen, *Appl. Catal. B: Environ.* **2008**, 81, 236-243.
[28] S. Jun, S. H. Joo, R. Ryoo, M Kruk, M. Jaroniec, Z. Liu, T. Ohsuna, O. Terasaki, *J. Am. Chem. Soc.* **2000**, 122, 10712-10713.
[29] W. Shen, X. Dong, Y. Zhu, H. Chen, J. Shi, *Micropor. Mesopor. Mat.* **2005**, 85, 157-162.
[30] Y. Su, L. Dai, Q. Zhang, Y. Li, J. Peng, R. a. Wu, W. Han, Z. Tang, Y. Wang, *Catal. Sur. Asia.* **2016**, 20, 231-240.
[31] Y. Su, Z. Tang, W. Han, Y. Song, G. Lu, *Catal. Sur. Asia.* **2015**, 19, 129-139.
[32] J. Zhao, Y. Zou, X. Zou, T. Bai, Y. Liu, R. Gao, D. Wang, G. D. Li, *Nanoscale.* **2014**, 6, 7255-7262.
[33] N.M. Deraz, *Appl. Surf. Sci.* **2009**, 255, 3884−3890.
[34] D. Larcher, G. Sudant, R. Patrice, J. M. Tarascon, *Chem. Mater.* **2003**, 15, 3543-3551.
[35] M. A. Henderson, C. L. Perkins, M. H. Engelhard, S. Thevuthasan, C. H. F. Peden, *Sur. Sci* **2003**, 526, 1-18.
[36] C. He, Y. Yu, L. Yue, N. Qiao, J. Li, Q. Shen, W. Yu, J. Chen, Z. Hao, *Appl. Catal. B: Environ.* **2014**, 147, 156-166.
[37] Y. Wang, F. Wang, Y. Chen, D. Zhang, B. Li, S. Kang, X. Li, L. Cui, *Appl. Catal. B: Environ.* **2014**, 147, 602-609.
[38] C.B. Gopl, M. Garcia-Melchor, S.C. Lee, Y.Z. Shi, A. Shavorskiy, M. Monti, Z.X. Guan, R. Sinclair, H. Bluhm, A. Vojvodic, W.C. Chueh, *Nat. commun.* **2017,** 8, 15360
[39] W. Shan, Z. Feng, Z. Li, J. Zhang, W. Shen, C. Li, *J. Catal.* **2004**, 228, 206-217.
[40] A. Gurbani, J. L. Ayastuy, M. P. González-Marcos, M. A. Gutiérrez-Ortiz, *Int. J. Hydrogen Energ*. **2010**, 35, 11582-11590.
[41] Y. Li, Q. Fu, M. Flyzani-Stephanopoulos, *Appl. Catal. B: Environ.* **2000**, 27, 179-191.
[42] B. Y. Bai, H. Arandiyan, J. H. Li, *Appl. Catal. B: Environ*. **2013**, 142-143, 677-683.
[43] B.P. Barbero, J.A. Gamboa, L.E. Cadus, *Appl. Catal. B: Environ.* **2006**, 65, 21-30.
[44] L. Xue, C. Zhang, H.He, Y. Teraoka, *Appl. Catal. B: Environ.* **2007**, 75, 167-174.
[45] Z. Q. Zou, M. Meng, Y. Q. Zha, *J. Phys. Chem. C.* **2010**, 114, 468-477.
[46] C. Ma, Z. Mu, J. Li, Y. Jin, J. Cheng, G. Lu, Z. Hao, S. Qiao, *J. Am. Chem. Soc,* **2010**, 132, 2608-2613.
[47] H. Mai, D. Zhang, L. Shi, T. Yan, H. Li, *Appl. Sur. Sci.* **2011**, 257, 7551-7559.
[48] Y.S. Xia, H.X. Dai, H.Y. Jiang, L.Zhang, J.G. Deng, Y.X. Liu, *J. Hazard. Mater*. **2011**, 186, 84-91.
[49] T. Montini, M. Melchionna, M. Monai, P. Fornasiero, *Chem. Rev*. **2016**, 116, 5987-6041.
[50] F. Yang, J. Wei, W. Liu, J. Guo, Y. Yang, *J. Mater. Chem. A.* **2014**, 2, 5662-5667.

10.1002/ejic.201800348

WILEY-VCH

Entry for the Table of Contents (Please choose one layout)

Layout 1:

FULL PAPER

Herein, we describe a facile template-free approach to synthesize hollow-hierarchically multiporous wall CeO_2 (HMW-CeO_2) nanospheres. The CuO loaded HMW-CeO_2 support (HMW-CuO@CeO_2) was evaluated for the catalytic activity in the CO oxidation reaction. The catalytic activity of HMW-CuO@CeO_2 remains unchanged after three cycles and no loss of CO conversion is observed after 12h on stream at 60 ºC.

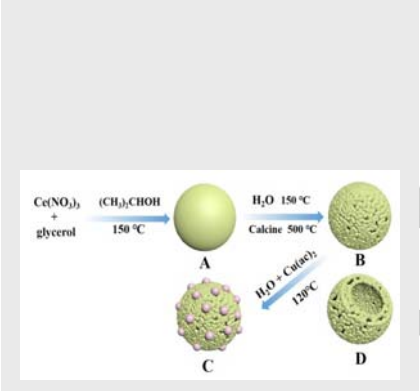

Yunfei Su[a,b], Shanshan Yuan[a,b], Dandan Ning[a,b], Qingwen Zhang[a,b], Weiliang Han[c] and Yi Wang[a,b]*

Page No. – Page No.

The template-free synthesis of CuO@CeO_2 nanospheres: facile strategy, structure optimization, and enhanced catalytic activity toward CO oxidation